PHYSICAL REVIEW B **92**, 180504(R) (2015)

Energy dependence of the spin excitation anisotropy in uniaxial-strained $BaFe_{1.9}Ni_{0.1}As_2$

Yu Song,[1] Xingye Lu,[1,2] D. L. Abernathy,[3] David W. Tam,[1] J. L. Niedziela,[4] Wei Tian,[3] Huiqian Luo,[2] Qimiao Si,[1] and Pengcheng Dai[1,*]

[1]*Department of Physics and Astronomy, Rice University, Houston, Texas 77005, USA*
[2]*Beijing National Laboratory for Condensed Matter Physics, Institute of Physics, Chinese Academy of Sciences, Beijing 100190, China*
[3]*Quantum Condensed Matter Division, Oak Ridge National Laboratory, Oak Ridge, Tennessee 37831, USA*
[4]*Instrument and Source Division, Oak Ridge National Laboratory, Oak Ridge, Tennessee 37831, USA*

(Received 22 August 2015; revised manuscript received 23 September 2015; published 6 November 2015)

We use inelastic neutron scattering to study the temperature and energy dependence of the spin excitation anisotropy in uniaxial-strained electron-doped iron pnictide $BaFe_{1.9}Ni_{0.1}As_2$ near optimal superconductivity ($T_c = 20$ K). Our work has been motivated by the observation of in-plane resistivity anisotropy in the paramagnetic tetragonal phase of electron-underdoped iron pnictides under uniaxial pressure, which has been attributed to a spin-driven Ising-nematic state or orbital ordering. Here we show that the spin excitation anisotropy, a signature of the spin-driven Ising-nematic phase, exists for energies below ~60 meV in uniaxial-strained $BaFe_{1.9}Ni_{0.1}As_2$. Since this energy scale is considerably larger than the energy splitting of the d_{xz} and d_{yz} bands of uniaxial-strained $Ba(Fe_{1-x}Co_x)_2As_2$ near optimal superconductivity, spin Ising-nematic correlations are likely the driving force for the resistivity anisotropy and associated electronic nematic correlations.

DOI: 10.1103/PhysRevB.92.180504 PACS number(s): 74.25.Ha, 74.25.Jb, 74.70.−b, 78.70.Nx

An electronic nematic phase, where the rotational symmetry of the system is spontaneously broken without breaking the translational symmetry of the underlying lattice [1], has been observed close to the superconducting phase in iron pnictides [2]. In the undoped state, the parent compounds of iron pnictide superconductors such as $BaFe_2As_2$ exhibit a tetragonal-to-orthorhombic structural transition at T_s that precedes the onset of long-range collinear antiferromagnetic (AF) order below the ordering temperature T_N [3–8]. Upon electron doping via partially replacing Fe by Co or Ni to form $Ba(Fe_{1-x}Co_x)_2As_2$ [9,10] or $BaFe_{2-x}Ni_xAs_2$ [11,12], both T_s and T_N are suppressed with increasing doping leading to superconductivity [Fig. 1(a)]. A key signature of electronic nematicity has been the in-plane resistivity anisotropy found in $Ba(Fe_{1-x}Co_x)_2As_2$ under uniaxial pressure above the superconducting transition temperature T_c, stress-free T_N and T_s [13–15]. In particular, recent elastoresistance [15–17] and elastic moduli [18,19] measurements on $Ba(Fe_{1-x}Co_x)_2As_2$ reveal a divergence of the electronic nematic susceptibility, defined as the susceptibility of electronic anisotropy to anisotropic in-plane strain, upon approaching T_s. While these results indicate that the structural phase transition is driven by electronic degrees of freedom, it is still unclear whether it is due to the spin Ising-nematic state that breaks the in-plane fourfold rotational symmetry of the underlying paramagnetic tetragonal lattice [20–25], or arises from the orbital ordering of Fe d_{xz} and d_{yz} orbitals among the five Fe 3d orbitals [26–30].

Experimentally, inelastic neutron scattering (INS) experiments on $BaFe_{2-x}Ni_xAs_2$ ($x = 0,0.085,0.12$) under uniaxial pressure indicate that spin excitations at energies below 16 meV change from fourfold symmetric to twofold symmetric in the tetragonal phase at temperatures approximately corresponding to the onset of the in-plane resistivity anisotropy, thus suggesting that the spin Ising-nematic correlations are associated with the resistivity anisotropy [31]. On the other hand, x-ray linear dichroism [32] and angle-resolved photoemission spectroscopy (ARPES) [33,34] experiments indicate the tendency towards orbital ordering in the tetragonal phase of $Ba(Fe_{1-x}Co_x)_2As_2$ under uniaxial pressure. In particular, an in-plane electronic anisotropy, characterized by a ~60 meV energy splitting of two orthogonal bands with dominant d_{xz} ($\mathbf{Q}_2$) and d_{yz} ($\mathbf{Q}_1$) character in the AF ordered orthorhombic state of undoped $BaFe_2As_2$ and underdoped $Ba(Fe_{1-x}Co_x)_2As_2$ [Figs. 1(c) and 1(d)], is observed to develop above the stress-free T_N and T_s similar to the resistivity anisotropy [Fig. 1(e)] [33]. Furthermore, the uniaxial pressure necessary to detwin $Ba(Fe_{1-x}Co_x)_2As_2$ or $BaFe_{2-x}Ni_xAs_2$ iron pnictides can also affect their transport properties [35], and magnetic [36,37] and structural [38] phase transitions. Therefore, it remains unclear if the electronic nematic phase is due to the spin Ising-nematic state [20–25], orbital ordering [26–30], or applied uniaxial strain via enhanced spin or orbital nematic susceptibility.

One way to reveal whether the spin Ising-nematic state is associated with orbital ordering or not is to determine the energy dependence of the spin excitation anisotropy and its electron-doping dependence. By determining the energy and temperature dependence of the spin excitation anisotropy, one can compare the outcome with temperature and electron-doping dependence of the energy splitting of the d_{xz} and d_{yz} bands in $Ba(Fe_{1-x}Co_x)_2As_2$ [33], and therefore establish whether and how the spin Ising-nematic correlations are associated with orbital ordering [39].

In this Rapid Communication, we report INS studies of temperature and energy evolution of the spin excitation anisotropy in superconducting $BaFe_{1.9}Ni_{0.1}As_2$ ($T_c = 20$ K, $T_N \approx T_s \approx 30 \pm 5$ K) detwinned under uniaxial pressure [12,40–43]. We chose to study $BaFe_{1.9}Ni_{0.1}As_2$ because ARPES measurements on $Ba(Fe_{1-x}Co_x)_2As_2$ samples reveal vanishing energy splitting of the d_{xz} and d_{yz} bands (~20 meV) and orbital ordering approaching optimal doping [33]. Using time-of-flight neutron spectroscopy, we show that the spin excitation anisotropy in $BaFe_{1.9}Ni_{0.1}As_2$ in the low-temperature superconducting

*pdai@rice.edu

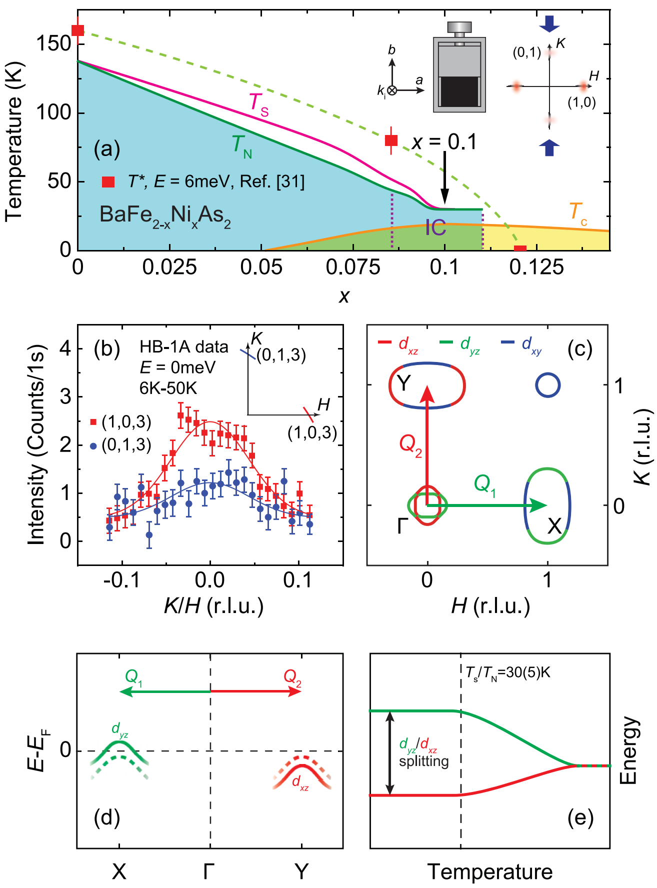

FIG. 1. (Color online) (a) The phase diagram of $BaFe_{2-x}Ni_xAs_2$. In $BaFe_{1.9}Ni_{0.1}As_2$ superconductivity coexists with incommensurate (IC) short-range magnetic order [11]. The mechanical clamp used and the magnetic excitations under uniaxial pressure along the b axis are schematically shown in the inset at the top right. The red squares and dashed line mark T^*, a crossover temperature at which the intensity of low-energy magnetic excitations at (1,0) and (0,1) in $BaFe_{2-x}Ni_xAs_2$ under uniaxial pressure merge [31]. (b) Rocking scans of the elastic magnetic peak at 6 K obtained on HB-1A; background measured at 50 K has been subtracted. The inset shows the rocking scans projected into the $[H,K,0]$ plane. (c) Schematic Fermi surface of $BaFe_{1.9}Ni_{0.1}As_2$ in the paramagnetic state; the arrows mark nesting wave vectors $\mathbf{Q}_1 = (1,0)$ and $\mathbf{Q}_2 = (0,1)$. Fermi surfaces originating from different orbitals are shown in different colors. (d) Schematic splitting of d_{yz} and d_{xz} bands at X and Y in $Ba(Fe_{1-x}Co_x)_2As_2$, as found by ARPES [33]. At higher temperatures, the two bands have the same energy (dashed lines) but as the temperature is lowered the d_{yz} band moves up in energy, whereas d_{xz} moves down. (e) Schematic temperature dependence of the orbital splitting in (d); under uniaxial pressure the splitting persists to above the stress-free T_N and T_s.

state decreases with increasing energy, and vanishes for energies above ~60 meV (Fig. 2). This anisotropy energy scale is remarkably similar to the energy splitting (~65 meV) of the d_{xz} and d_{yz} bands seen by ARPES in the undoped and electron underdoped $Ba(Fe_{1-x}Co_x)_2As_2$ iron pnictides [Fig. 1(e)] [33]. Upon warming to high temperatures, the spin excitation anisotropy at $E = 4.5 \pm 0.5$ meV decreases smoothly with increasing temperature showing no anomaly across T_c, stress-free T_N and T_s, and vanishes around a crossover temperature T^*, where resistivity anisotropy vanishes (Fig. 3) [31]. The

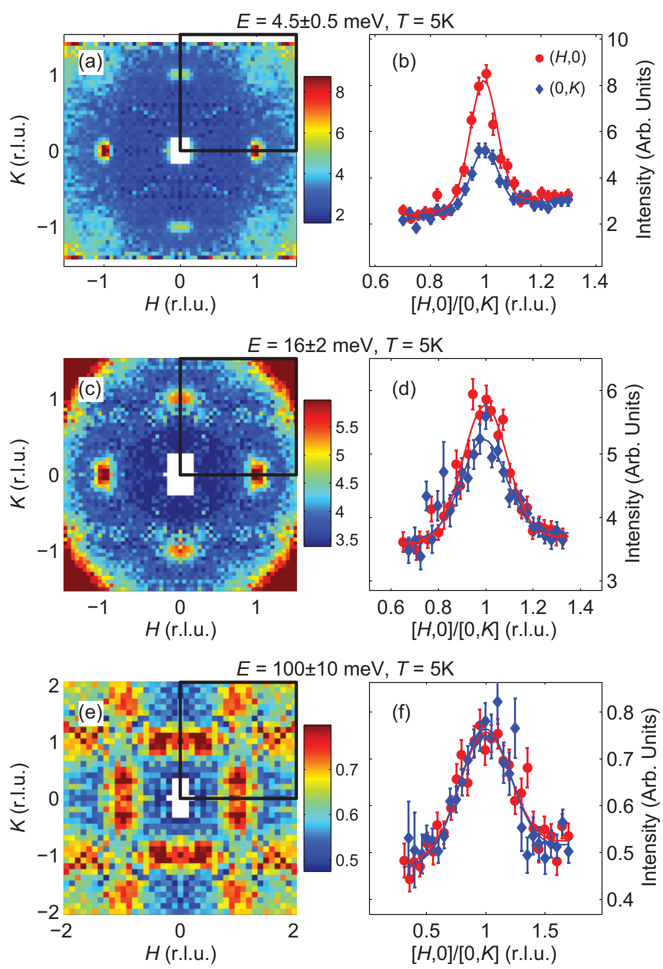

FIG. 2. (Color online) Constant-energy slices symmetrized along H and K axes at $T = 5$ K for energy transfers (a) $E = 4.5 \pm 0.5$ meV ($E_i = 30$ meV), (c) $E = 16 \pm 2$ meV ($E_i = 80$ meV), and (e) $E = 100 \pm 10$ meV ($E_i = 250$ meV). The black boxes indicate regions that contain nonduplicate data due to symmetrizing. Longitudinal cuts along $[H,0]$ (red circles) and $[0,K]$ (blue diamonds) for energy transfers in (a), (c), and (e) are, respectively, shown in (b), (d), and (f). The solid lines are fits using Gaussian functions and linear backgrounds. $[H,0]/[0,K]$ scans are obtained by binning K/H in the range (b) $[-0.15,0.15]$, (d) $[-0.175,0.175]$, and (f) $[-0.3,0.3]$ after folding along K/H axis.

energy dependence of the spin excitation anisotropy, however, is weakly temperature dependent from 5 K ($\ll T_c$) to 35 K ($> T_N, T_s$), and persists below 60 meV. Since the energy splitting of the d_{xz} and d_{yz} orbitals decreases with increasing electron doping for $Ba(Fe_{1-x}Co_x)_2As_2$ and diminishes rapidly above T_N [33], our observation of the large energy (~60 meV) spin excitation anisotropy in the uniaxial strained paramagnetic state of a nearly optimally electron doped $BaFe_{1.9}Ni_{0.1}As_2$ is larger than the energy splitting of the Fe d_{xz} and d_{yz} bands for optimally doped iron pnictides above T_N, thus suggesting that the spin Ising-nematic state may be the driving force for the electronic nematicity in iron pnictides [20–25].

Our neutron scattering experiments were carried out at the wide angular-range chopper spectrometer (ARCS) at the Spallation Neutron Source and HB-1A triple-axis spectrometer

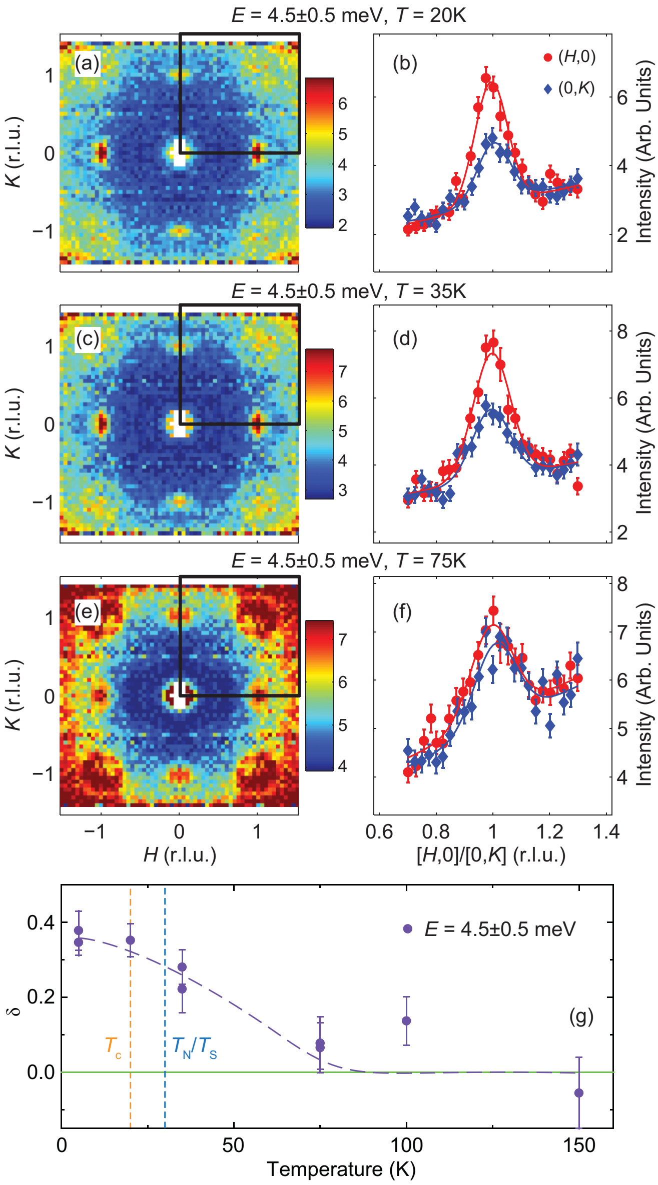

FIG. 3. (Color online) Constant-energy slices symmetrized along H and K axes for $E = 4.5 \pm 0.5$ meV ($E_i = 30$ meV) at (a) 20 K, (c) 35 K, and (e) 75 K. Corresponding longitudinal cuts along $[H,0]$ (red circles) and $[0,K]$ (blue diamonds) are respectively shown in (b), (d), and (f). $[H,0]/[0,K]$ scans are obtained by binning K/H in the range $[-0.15,0.15]$ after folding along K/H axis. (g) Temperature dependence of the anisotropy $\delta = (I_{10} - I_{01})/(I_{10} + I_{01})$ for $E = 4.5 \pm 0.5$ meV. The purple dashed line is a guide to the eye. T_c and stress-free T_N/T_s are marked by vertical dashed lines.

at the High-Flux Isotope Reactor, Oak Ridge National Laboratory. The $BaFe_{1.9}Ni_{0.1}As_2$ single crystals [40,41] are cut along the a and b axes and each cut sample is loaded into an individual mechanical clamp with applied uniaxial pressure [44]. 9 crystals with a total mass of 6.5 grams were coaligned. Elastic neutron scattering measurements were carried out on HB-1A to determine the detwinning ratio in the orthorhombic phase. The momentum transfer $\mathbf{Q}$ in three-dimensional reciprocal space in Å^{-1} is defined as $\mathbf{Q} = H\mathbf{a}^* + K\mathbf{b}^* + L\mathbf{c}^*$, where H, K, and L are Miller indices and $\mathbf{a}^* = \hat{\mathbf{a}}2\pi/a$, $\mathbf{b}^* = \hat{\mathbf{b}}2\pi/b$, $\mathbf{c}^* = \hat{\mathbf{c}}2\pi/c$ with $a \approx b = 5.564$ Å, and $c = 12.77$ Å. In the AF ordered state of a fully detwinned sample, the AF Bragg peaks should occur at $(\pm1,0,L)$ $(L = 1,3,5,\ldots)$ positions in reciprocal space [7]. For elastic neutron scattering measurements on HB-1A, the samples are aligned in the scattering plane spanned by the wave vectors (1,0,3) and (0,1,3) with $E_i = 14.6$ meV. Figure 1(b) shows elastic scans through the (1,0,3) and (0,1,3) positions to obtain the ratio ($R = I_{10}/I_{01}$) of magnetic intensities. Two Gaussians with linear backgrounds having the same widths and backgrounds were fit to scans as solid lines [Fig. 1(b)]. Anisotropy of intensities between $\mathbf{Q}_1 = (1,0)$ and $\mathbf{Q}_2 = (0,1)$ is then obtained through $\delta = (I_{10} - I_{01})/(I_{10} + I_{01}) = (R - 1)/(R + 1) \approx 0.5$. In a fully detwinned sample, one would expect $\delta \to 1$, while in a completely twinned sample $\delta \to 0$. In a partially detwinned sample with volume fraction of x corresponding to magnetic order at (1,0), the actual observed spin excitation intensities at (1,0) and (0,1) should, respectively, be $I_{10} = x\widetilde{I}_{10} + (1-x)\widetilde{I}_{01}$ and $I_{01} = x\widetilde{I}_{01} + (1-x)\widetilde{I}_{10}$, with $\widetilde{I}_{10}$ and $\widetilde{I}_{01}$ being the spin excitation intensity at (1,0) and (1,0) in a fully detwinned sample. Therefore, for a partially detwinned sample, one has $\delta = (I_{10} - I_{01})/(I_{10} + I_{01}) = (2x - 1)\widetilde{\delta}$ with $\widetilde{\delta} = (\widetilde{I}_{10} - \widetilde{I}_{01})/(\widetilde{I}_{10} + \widetilde{I}_{01})$. This means that regardless of the detwinning ratio, δ is directly proportional to $\widetilde{\delta}$ and the energy/temperature dependence of experimentally obtained δ display the intrinsic behavior of $\widetilde{\delta}$ even for a partially detwinned sample. For the ARCS experiment, incident beam is directed along the c axis of the samples and incident energies of $E_i = 30$, 80, 150, and 250 meV were used. The observed magnetic scatterings I_{10} and I_{01} are related to the imaginary part of the dynamic susceptibility χ''_{10} and χ''_{01}, respectively, via the Bose factor [5].

Figures 2(a), 2(c), and 2(e) show constant-energy slices of spin excitations in $BaFe_{1.9}Ni_{0.1}As_2$ in the (H,K) plane at 5 K for energy transfers $E = 4.5 \pm 0.5$, 16 ± 2, and 100 ± 10 meV, respectively. For $E = 4.5 \pm 0.5$ meV, the scattering intensity at $\mathbf{Q}_1 = (\pm1,0)$ is much stronger than at $\mathbf{Q}_2 = (0,\pm1)$ [Fig. 2(a)] [31]. Figure 2(b) compares constant-energy cuts along the $[H,0]$ and $[0,K]$ directions, confirming the stronger intensity at (1,0). On increasing the energy to $E = 16 \pm 2$ meV, the intensity difference between $\mathbf{Q}_1 = (\pm1,0)$ and $\mathbf{Q}_2 = (0,\pm1)$ becomes smaller [Fig. 2(c)], as revealed in constant-energy cuts of Fig. 2(d). At an energy transfer of $E = 100 \pm 10$ meV, the scattering becomes isotropic, and no discernible difference can be seen at $\mathbf{Q}_1 = (\pm1,0)$ and $\mathbf{Q}_2 = (0,\pm1)$ [Fig. 2(e)]. This is confirmed by constant-energy cuts along the $[H,0]$ and $[0,K]$ directions [Fig. 2(f)].

Figure 3 shows constant-energy slices of spin excitations with $E = 4.5 \pm 0.5$ meV on warming from $T = 20$ to 75 K. At $T = 20$ K ($T_s \geqslant T_N > T > T_c$), the spin excitation anisotropy shown in Figs. 3(a) and 3(b) is similar to $T = 5$ K [Figs. 2(a) and 2(b)]. On warming to $T = 35$ K ($T > T_s \geqslant T_N > T_c$) corresponding to the tetragonal state in stress-free samples, clear differences in spin excitation intensity between $\mathbf{Q}_1 = (\pm1,0)$ and $\mathbf{Q}_2 = (0,\pm1)$ can still be seen [Figs. 3(c) and 3(d)]. The differences between these two wave vectors essentially disappear at $T = 75$ K, a temperature well above the strain-free T_s and T_N [Figs. 3(e) and 3(f)]. The spin excitation anisotropy δ decreases smoothly with increasing temperature

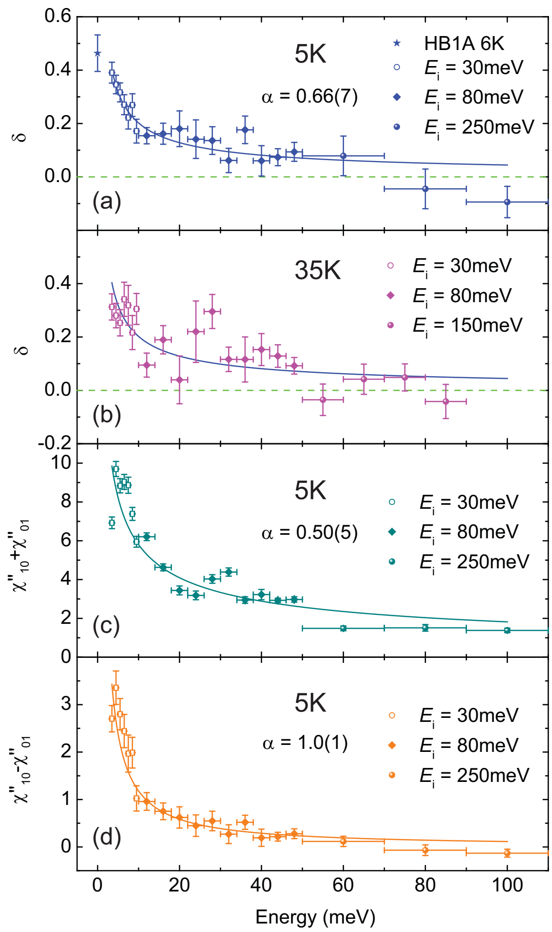

FIG. 4. (Color online) Energy dependence of anisotropy between $\mathbf{Q}_1$ and $\mathbf{Q}_2$ defined as $\delta = (I_{10} - I_{01})/(I_{10} + I_{01})$ for (a) 5 K and (b) 35 K. (c) Energy dependence of $\chi''_{10} + \chi''_{01}$ at 5 K; χ''_{10} and χ''_{01} are dynamic susceptibilities at $\mathbf{Q}_1 = (1,0)$ and $\mathbf{Q}_2 = (0,1)$. (d) $\chi''_{10} - \chi''_{01}$. Data obtained on HB-1A is collected at 6 K, and is plotted together with ARCS data using incident energies $E_i = 30$, 80, 150, and 250 meV. It should be noted that below 10 meV magnetic excitations have significant L-modulation. Since E and L are coupled for our scattering geometry, the strong enhancement in (c) and (d) below 10 meV is in part due to L-modulation. The resonance mode in the superconducting state also contributes to the enhancement below 10 meV. However, given that the anisotropy (δ) does not depend on absolute intensity, δ in (a) reflects instrinsic properties of the system regardless of L-modulation.

and vanishes around 80 K [Fig. 3(g)], similar to the resistivity anisotropy [31].

To quantitatively determine the energy and temperature dependence of spin excitation anisotropy, we systematically made constant-energy slices and cuts along $[H,0]$ and $[0,K]$ at various energies similar to Figs. 2 and 3. Based on the cuts, we can estimate the energy dependence of the spin excitation anisotropy δ [44]. Figure 4(a) shows that the spin excitation anisotropy (δ) decreases with increasing energy and vanishes for energy transfers above ~60 meV at $T = 5$ K ($\ll T_c, T_N, T_s$). On warming to 35 K, a temperature above T_c, T_N, and T_s, the energy of the spin excitation anisotropy still persists to about ~60 meV, similar to 5 K [Fig. 4(b)].

We are now in a position to compare and contrast our results with the orbital ordering tendencies indicated by the ARPES measurements [33]. The energy splitting of the d_{xz} and d_{yz} bands in undoped and underdoped $Ba(Fe_{1-x}Co_x)_2As_2$ is also about ~60 meV, and is likewise weakly temperature dependent below T_s [Fig. 1(e)] [33]. Upon increasing the doping level to near optimal superconductivity, the ARPES-measured orbital splitting energy in electron-doped iron pnictides decreases to ~20 meV and vanishes very rapidly above T_N, T_s [33]. Since the ARPES-measured orbital splitting energy [33] and neutron scattering measured spin excitation anisotropy [31] in the paramagnetic state may be uniaxial strain dependent [35], it would be more constructive to compare the doping dependence of the spin excitation anisotropy in the uniaxial strained paramagnetic state with those of ARPES measurements. For $BaFe_2As_2$, our unpublished results suggest spin excitation anisotropy persists to about 60 meV at 145 K (just above T_N, T_s of 138 K). For $BaFe_{1.9}Ni_{0.1}As_2$, δ is also nonzero below ~60 meV both below and above T_N, T_s [Figs. 4(a) and 4(b)]. This means that spin excitations anisotropy is weakly doping dependent and has a larger anisotropy energy scale than that of the ARPES-measured orbital splitting energy, suggesting that it is likely the spin channel, instead of the orbital sector, that drives the Ising-nematic correlations.

To further analyze the energy dependence of the spin correlations, we show in Figs. 4(c) and 4(d) the energy dependence of the sum, $\chi''_{10} + \chi''_{01}$, and difference, $\chi''_{10} - \chi''_{01}$, of the dynamic susceptibilities at the two wave vectors [For the measured energy and temperature range, $\chi''(\mathbf{Q},\omega)$ is directly proportional to the measured neutron scattering intensity assuming the magnetism is essentially two dimensional and after correcting for the magnetic form factor], respectively. It is seen that both quantities increase as energy is decreased. Within the measured energy range, both the sum and difference can be fit with a power-law dependence on the energy, $\sim 1/E^{\alpha}$, with exponents α being 0.50(5) and 1.0(1), respectively. The ratio, δ, can also be fitted with a power-law divergence, although this divergence must be truncated at frequencies below the measured low-frequency limit, because δ must be bound by 1. Overall, our data on the sum, $\chi''_{10} + \chi''_{01}$ [Fig. 4(c)], are in general agreement with results of the previous studies on twinned samples [45,46], which fitted the spectra using a model form for the dynamical spin susceptibility $\chi'' \sim E/(E^2 + \Gamma^2) \sim 1/E^{\alpha}$ with $\alpha = 1$ if $\Gamma \to 0$. In our work, we show that the difference, $\chi''_{10} - \chi''_{01}$ [Fig. 4(d)], behaves similarly. Within the description of the spin-driven Ising-nematic correlations, the quantum critical behavior in the spin and nematic correlations has been anticipated theoretically [21]. We should caution that the precise values of the exponents are uncertain, because the data below 10 meV is affected by the L-modulation and, for $T < T_c$, by superconductivity.

It is instructive to contrast the spin nematic scenario with an alternative picture based on orbital ordering. Since the electron-doping evolution of the low-energy spin excitations in $BaFe_{2-x}Ni_xAs_2$ is consistent with quasiparticle excitations between the hole Fermi surfaces near Γ and electron Fermi surfaces at $\mathbf{Q}_1 = (1,0)$ [$\mathbf{Q}_2 = (0,1)$] [Fig. 1(c)] [47], an energy splitting of the d_{xz} and d_{yz} bands at these two wave vectors should result in spin excitation anisotropy as seen by

INS [39]. However, this picture would require that the tendency towards the orbital ordering is stronger than the spin-excitation anisotropy, which is opposite to our results near the optimal electron doping. Nevertheless, since spin and orbital degrees of freedom in iron pnictides are generally coupled, it may not be experimentally possible to conclusively determine if spin or orbital degrees of freedom is the driving force for the enhanced nematic susceptibility.

In summary, we have discovered that the fourfold symmetric to twofold symmetric transition of spin excitations in $BaFe_{2-x}Ni_xAs_2$ under uniaxial pressure is energy dependent and occurs for energy transfers below about 60 meV in near optimally electron-doped iron pnictides. Since orbital splitting becomes vanishingly small for optimally electron-doped iron pnictides in the paramagnetic state of the uniaxial strained sample, our results would suggest that the spin excitation anisotropy or spin Ising-nematic correlations are the driving force for the electronic nematic correlations in iron pnictides.

The neutron scattering work at Rice is supported by the U.S. NSF DMR-1362219 and DMR-1436006 (P.D.). This work is also supported by the Robert A. Welch Foundation Grants No. C-1839 (P.D.) and No. C-1411 (Q.S.). Q.S. is supported by the U.S. NSF DMR-1309531. The neutron scattering work at ORNL's HFIR and SNS was sponsored by the Scientific User Facilities Division, Office of Basic Energy Sciences, U.S. Department of Energy. The work at IOP, CAS in China is supported by the NSFC Program (No. 11374011) and CAS (SPRP-B: XDB07020300).

[1] E. Fradkin, S. A. Kivelson, M. J. Lawler, J. P. Eisenstein, and A. P. Mackenzie, Annu. Rev. Condens. Matter Phys. **1**, 153 (2010).

[2] I. R. Fisher, L. Degiorgi, and Z. X. Shen, Rep. Prog. Phys. **74**, 124506 (2011).

[3] Y. Kamihara, T. Watanabe, M. Hirano, and H. Hosono, J. Am. Chem. Soc. **130**, 3296 (2008).

[4] G. R. Stewart, Rev. Mod. Phys. **83**, 1589 (2011).

[5] P. C. Dai, Rev. Mod. Phys. **87**, 855 (2015).

[6] C. de La Cruz, Q. Huang, J. W. Lynn, Jiying Li, W. Ratcliff II, J. L. Zarestky, H. A. Mook, G. F. Chen, J. L. Luo, N. L. Wang, and P. C. Dai, Nature (London) **453**, 899 (2008).

[7] Q. Huang, Y. Qiu, Wei Bao, M. A. Green, J. W. Lynn, Y. C. Gasparovic, T. Wu, G. Wu, and X. H. Chen, Phys. Rev. Lett. **101**, 257003 (2008).

[8] M. G. Kim, R. M. Fernandes, A. Kreyssig, J. W. Kim, A. Thaler, S. L. Bud'ko, P. C. Canfield, R. J. McQueeney, J. Schmalian, and A. I. Goldman, Phys. Rev. B **83**, 134522 (2011).

[9] C. Lester, J.-H. Chu, J. G. Analytis, S. C. Capelli, A. S. Erickson, C. L. Condron, M. F. Toney, I. R. Fisher, and S. M. Hayden, Phys. Rev. B **79**, 144523 (2009).

[10] S. Nandi, M. G. Kim, A. Kreyssig, R. M. Fernandes, D. K. Pratt, A. Thaler, N. Ni, S. L. Bud'ko, P. C. Canfield, J. Schmalian, R. J. McQueeney, and A. I. Goldman, Phys. Rev. Lett. **104**, 057006 (2010).

[11] H. Q. Luo, R. Zhang, M. Laver, Z. Yamani, M. Wang, X. Y. Lu, M. Y. Wang, Y. C. Chen, S. L. Li, S. Chang, J. W. Lynn, and P. C. Dai, Phys. Rev. Lett. **108**, 247002 (2012).

[12] X. Y. Lu, H. Gretarsson, R. Zhang, X. Liu, H. Q. Luo, W. Tian, M. Laver, Z. Yamani, Y.-J. Kim, A. H. Nevidomskyy, Q. Si, and P. C. Dai, Phys. Rev. Lett. **110**, 257001 (2013).

[13] J. H. Chu, J. G. Analytis, K. De Greve, P. L. McMahon, Z. Islam, Y. Yamamoto, and I. R. Fisher, Science **329**, 824 (2010).

[14] M. A. Tanatar, E. C. Blomberg, A. Kreyssig, M. G. Kim, N. Ni, A. Thaler, S. L. Bud'ko, P. C. Canfield, A. I. Goldman, I. I. Mazin, and R. Prozorov, Phys. Rev. B **81**, 184508 (2010).

[15] J. H. Chu, H.-H. Kuo, J. G. Analytis, and I. R. Fisher, Science **337**, 710 (2012).

[16] H.-H. Kuo and I. R. Fisher, Phys. Rev. Lett. **112**, 227001 (2014).

[17] H.-H. Kuo, J.-H. Chu, S. A. Kivelson, and I. R. Fisher, arXiv:1503.00402.

[18] M. Yoshizawa, D. Kimura, T. Chiba, S. Simayi, Y. Nakanishi, K. Kihou, C.-H. Lee, A. Iyo, H. Eisaki, M. Nakajima, and S. Uchida, J. Phys. Soc. Jpn. **81**, 024604 (2012).

[19] A. E. Böhmer, P. Burger, F. Hardy, T. Wolf, P. Schweiss, R. Fromknecht, M. Reinecker, W. Schranz, and C. Meingast, Phys. Rev. Lett. **112**, 047001 (2014).

[20] P. Chandra, P. Coleman, and A. I. Larkin, Phys. Rev. Lett. **64**, 88 (1990).

[21] J. Dai, Q. Si, J. X. Zhu, and E. Abrahams, Proc. Natl. Acad. Sci. USA **106**, 4118 (2009).

[22] J. P. Hu and C. K. Xu, Physica C **481**, 215 (2012).

[23] R. M. Fernandes, A. V. Chubukov, and J. Schmalian, Nat. Phys. **10**, 97 (2014).

[24] R. M. Fernandes, A. V. Chubukov, J. Knolle, I. Eremin, and J. Schmalian, Phys. Rev. B **85**, 024534 (2012).

[25] R. M. Fernandes and J. Schmalian, Supercond. Sci. Technol. **25**, 084005 (2012).

[26] C. C. Lee, W. G. Yin, and W. Ku, Phys. Rev. Lett. **103**, 267001 (2009).

[27] F. Krüger, S. Kumar, J. Zaanen, and J. van den Brink, Phys. Rev. B **79**, 054504 (2009).

[28] W. C. Lv, J. S. Wu, and P. Phillips, Phys. Rev. B **80**, 224506 (2009).

[29] C.-C. Chen, J. Maciejko, A. P. Sorini, B. Moritz, R. R. P. Singh, and T. P. Devereaux, Phys. Rev. B **82**, 100504(R) (2010).

[30] B. Valenzuela, E. Bascones, and M. J. Calderón, Phys. Rev. Lett. **105**, 207202 (2010).

[31] X. Y. Lu, J. T. Park, R. Zhang, H. Q. Luo, A. N. Nevidomskyy, Q. Si, and P. C. Dai, Science **345**, 657 (2014).

[32] Y. K. Kim, W. S. Jung, G. R. Han, K.-Y. Choi, C.-C. Chen, T. P. Devereaux, A. Chainani, J. Miyawaki, Y. Takata, Y. Tanaka, M. Oura, S. Shin, A. P. Singh, H. G. Lee, J.-Y. Kim, and C. Kim, Phys. Rev. Lett. **111**, 217001 (2013).

[33] M. Yi, D. H. Lu, J. H. Chu, J. G. Analytis, A. P. Sorini, A. F. Kemper, B. Moritz, R. G. Moore, M. Hashimoto, W. S. Lee, Z. Hussain, T. P. Devereaux, I. R. Fisher, and Z. X. Shen, Proc. Natl. Acad. Sci. USA **108**, 6878 (2011).

[34] Y. Zhang, C. He, Z. R. Ye, J. Jiang, F. Chen, M. Xu, Q. Q. Ge, B. P. Xie, J. Wei, M. Aeschlimann, X. Y. Cui, M. Shi, J. P. Hu, and D. L. Feng, Phys. Rev. B **85**, 085121 (2012).

[35] H. R. Man, X. Y. Lu, J. S. Chen, R. Zhang, W. L. Zhang, H. Q. Luo, J. Kulda, A. Ivanov, T. Keller, E. Morosan, Q. Si, and P. C. Dai, Phys. Rev. B **92**, 134521 (2015).

[36] C. Dhital, Z. Yamani, W. Tian, J. Zeretsky, A. S. Sefat, Z. Q. Wang, R. J. Birgeneau, and S. D. Wilson, Phys. Rev. Lett. **108**, 087001 (2012).

[37] C. Dhital, T. Hogan, Z. Yamani, R. J. Birgeneau, W. Tian, M. Matsuda, A. S. Sefat, Z. Wang, and S. D. Wilson, Phys. Rev. B **89**, 214404 (2014).

[38] X. Y. Lu, T. Keller, W. L. Zhang, Y. Song, J. T. Park, H. Q. Luo, S. L. Li, and P. C. Dai, arXiv:1507.04191.

[39] M. Kovacic, M. H. Christensen, M. N. Gastiasoro, and B. M. Andersen, Phys. Rev. B **91**, 064424 (2015).

[40] M. S. Liu, L. W. Harriger, H. Q. Luo, M. Wang, R. A. Ewings, T. Guidi, H. Park, K. Haule, G. Kotliar, S. M. Hayden, and P. C. Dai, Nat. Phys. **8**, 376 (2012).

[41] X. Y. Lu, D. W. Tam, C. L. Zhang, H. Q. Luo, M. Wang, R. Zhang, L. W. Harriger, T. Keller, B. Keimer, L.-P. Regnault, T. A. Maier, and P. C. Dai, Phys. Rev. B **90**, 024509 (2014).

[42] M. S. da Luz, J. J. Neumeier, R. K. Bollinger, A. S. Sefat, M. A. McGuire, R. Jin, B. C. Sales, and D. Mandrus, Phys. Rev. B **79**, 214505 (2009).

[43] S. Simayi, K. Sakano, H. Takezawa, M. Nakamura, Y. Nakanishi, K. Kihou, M. Nakajima, C.-H. Lee, A. Iyo, H. Eisaki, S. Uchida, and M. Yoshizawa, J. Phys. Soc. Jpn. **82**, 114604 (2013).

[44] See Supplemental Material at http://link.aps.org/supplemental/10.1103/PhysRevB.92.180504 for details in data analysis.

[45] D. S. Inosov, J. T. Park, P. Bourges, D. L. Sun, Y. Sidis, A. Schneidewind, K. Hradil, D. Haug, C. T. Lin, B. Keimer, and V. Hinkov, Nat. Phys. **6**, 178 (2010).

[46] K. Matan, S. Ibuka, R. Morinaga, Songxue Chi, J. W. Lynn, A. D. Christianson, M. D. Lumsden, and T. J. Sato, Phys. Rev. B **82**, 054515 (2010).

[47] H. Q. Luo, Z. Yamani, Y. C. Chen, X. Y. Lu, M. Wang, S. L. Li, T. A. Maier, S. Danilkin, D. T. Adroja, and P. C. Dai, Phys. Rev. B **86**, 024508 (2012).